



# Pulmonary myeloid cell uptake of biodegradable nanoparticles conjugated with an anti-fibrotic agent provides a novel strategy for treating chronic allergic airways disease

DOI:

[10.1016/j.biomaterials.2021.120796](https://doi.org/10.1016/j.biomaterials.2021.120796)

## Document Version

Accepted author manuscript

[Link to publication record in Manchester Research Explorer](#)

## Citation for published version (APA):

Chakraborty, A., Pinar, A. A., Lam, M., Bourke, J. E., Royce, S. G., Selomulya, C., & Samuel, C. S. (2021). Pulmonary myeloid cell uptake of biodegradable nanoparticles conjugated with an anti-fibrotic agent provides a novel strategy for treating chronic allergic airways disease. *Biomaterials*, 273, Article 120796. <https://doi.org/10.1016/j.biomaterials.2021.120796>

## Published in:

Biomaterials

## Citing this paper

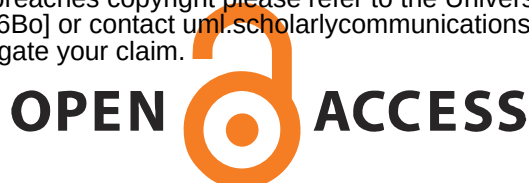
Please note that where the full-text provided on Manchester Research Explorer is the Author Accepted Manuscript or Proof version this may differ from the final Published version. If citing, it is advised that you check and use the publisher's definitive version.

## General rights

Copyright and moral rights for the publications made accessible in the Research Explorer are retained by the authors and/or other copyright owners and it is a condition of accessing publications that users recognise and abide by the legal requirements associated with these rights.

## Takedown policy

If you believe that this document breaches copyright please refer to the University of Manchester's Takedown Procedures [<http://man.ac.uk/04Y6Bo>] or contact [um.scholarlycommunications@manchester.ac.uk](mailto:um.scholarlycommunications@manchester.ac.uk) providing relevant details, so we can investigate your claim.



# Pulmonary myeloid cell uptake of biodegradable nanoparticles conjugated with an anti-fibrotic agent provides a novel strategy for treating chronic allergic airways disease

*Amlan Chakraborty<sup>1,2</sup>, Anita A. Pinar<sup>1</sup>, Maggie Lam<sup>1</sup>, Jane E. Bourke<sup>1</sup>, Simon G. Royce<sup>1,3</sup>, Cordelia Selomulya<sup>4,\*</sup> and Chrishan S. Samuel<sup>1,5,\*</sup>.*

<sup>1</sup>Monash Biomedicine Discovery Institute and Department of Pharmacology, Monash University, Clayton, Victoria, Australia. <sup>2</sup>Department of Chemical Engineering, Monash University, Clayton, Victoria, Australia. <sup>3</sup>Department of Clinical Pathology and Department of Paediatrics, The University of Melbourne, Parkville, Victoria, Australia. <sup>4</sup>School of Chemical Engineering, UNSW Sydney, New South Wales, Australia; <sup>5</sup>Department of Biochemistry and Molecular Biology, The University of Melbourne, Parkville, Victoria, Australia.

**\*Professor Cordelia Selomulya,**

School of Chemical Engineering,

UNSW Sydney,

Sydney, New South Wales 2052, Australia.

Tel: +612 9385 6243 / Email: cordelia.selomulya@unsw.edu.au

**\*Professor Chrishan S. Samuel,**

Monash Biomedicine Discovery Institute and Department of Pharmacology,

Monash University,

Clayton, Victoria 3800, Australia.

Tel: +613 9902 0152 / Email: chrishan.samuel@monash.edu

## ABSTRACT

Asthma (chronic allergic airways disease, AAD) is characterized by airway inflammation (AI), airway remodeling (AWR) and airway hyperresponsiveness (AHR). Current treatments for AAD mainly focus on targeting AI and its contribution AHR, with the use of corticosteroids. However, there are no therapies for the direct treatment of AWR, which can contribute to airway obstruction, AHR and corticosteroid resistance independently of AI. The acute heart failure drug, serelaxin (recombinant human gene-2 relaxin, RLX), has potential anti-remodelling and anti-fibrotic effects but only when continuously infused or injected to overcome its short half-life. To alleviate this limitation, we conjugated serelaxin to biodegradable and noninflammatory nanoparticles (NP-RLX) and evaluated their therapeutic potential on measures of AI, AWR and AHR, when intranasally delivered to a preclinical rodent model of chronic AAD and TGF- $\beta$ 1-stimulated collagen gel contraction from asthma patient-derived myofibroblasts. NP-RLX was preferentially taken-up by CD206<sup>+</sup>-infiltrating and CD68<sup>+</sup>-tissue resident alveolar macrophages. Furthermore, NP-RLX ameliorated the chronic AAD-induced AI, pro-inflammatory cytokines (IL-1 $\beta$ , IL-6, TNF- $\alpha$ ), chemokines (CCL2, CCL11) and the pro-fibrotic TGF- $\beta$ 1/IL-1 $\beta$  axis on AWR and resulting AHR, as well as human myofibroblast-induced collagen gel contraction, to a similar extent as unconjugated RLX. Hence, NP-RLX represents a novel strategy for treating the central features of asthma.

## INTRODUCTION

Asthma affects over 300 million people worldwide,<sup>1-3</sup> and is characterized by three interrelated pathological processes, comprising chronic airway inflammation (AI; influx of immune cells which release pro-inflammatory mediators), airway remodeling (AWR; airway structural changes) and airway hyperresponsiveness (AHR, the key clinical feature of asthma)<sup>1-4</sup>. These features are predominantly promoted by infiltrating T helper type-2 (Th2) cells and eosinophils that are responsible for inflammatory cell reactions that release pro-inflammatory mediators. The prolonged activation of these mediators in turn can result in aberrant AWR, leading to reticular basement membrane thickening and peri-bronchial fibrosis<sup>4-6</sup>. Clinically-used corticosteroids are effectively used to inhibit AI and its contribution to AHR<sup>4,7,8</sup>. However, a subset (~5-10%) of asthma sufferers are resistant to corticosteroids<sup>4,9,10</sup>. Hence, a therapy that ameliorates AI and AWR is essential, as the latter is associated with disease severity and steroid resistance.

The pleiotropic hormone-based drug, serelaxin (RLX; recombinant human gene H2-relaxin), has been demonstrated to markedly reduce established AWR and AHR, mainly through its anti-fibrotic<sup>2,11</sup> and bronchodilatory<sup>12,13</sup> properties in the setting of chronic AAD. Systemic administration of RLX by osmotic pump infusion<sup>11,14</sup> or daily intranasal administration<sup>15</sup> has consistently demonstrated its therapeutic effects, albeit requiring continuous/frequent administration to overcome its short half-life (minutes)<sup>16</sup>. Hence, there is a need for the sustained bioavailability of RLX to maintain its therapeutic efficacy in the airways/lung. These effects of RLX are mediated through its cognate G protein-coupled receptor, Relaxin Family Peptide Receptor 1 (RXFP1)<sup>17</sup>. While recent studies have suggested that RLX may modulate macrophages in other disease settings<sup>18</sup>, the potential regulation of these cells by RLX in the setting of chronic AAD/asthma remains poorly understood.

Previously, we have demonstrated that glycine conjugated super-paramagnetic iron oxide nanoparticles (SPIONs) are capable of being intranasally-delivered to target inflammatory cells within the inflamed lung<sup>19</sup>. SPIONs are biodegradable nanoparticles that can last in the lung for 48 hours before being broken down by endosomes<sup>20</sup> and are non-cytotoxic<sup>21</sup>. Herein, we demonstrate for the first time RLX-conjugated SPIONs (hereafter denoted as nanoparticle (NP)-RLX) as a carrier to maintain RLX activity, and which provide a novel tool for studying the uptake of RLX by myeloid cell subsets in the airways/lung. The Retention of NP-RLX in the lung for 48 hours without further accumulation, potentially enables prolonged RLX activity at the site of inflammation.

In the current study, we characterized the nature and activity of NP-RLX and demonstrated their selective uptake by infiltrating CD206<sup>+</sup> M2 macrophages and tissue-resident CD68<sup>+</sup> macrophages under inflammatory conditions. NP-RLX showed efficacy in attenuating AI, AWR (including fibrosis) and AHR when administered intranasally to a murine model of chronic AAD. NP-RLX also prevented TGF- $\beta$ 1-induced contraction of collagen gels seeded with human airway myofibroblasts obtained from patients with asthma. These results demonstrate a novel efficacious means of delivering a therapy for treating the AI, AWR and AHR associated with chronic AAD, and provide new knowledge on how the regulation of specific immune cell subsets in the airways/lung contributes to reducing the cardinal features of asthma.

## **METHODS**

### **Materials**

Iron (II) chloride tetrahydrate (puriss. p.a.,  $\geq 99.0\%$  (RT), Cat No. 44939), Iron (III) chloride hexahydrate (puriss. p.a., Reag. Ph. Eur.,  $\geq 99\%$ , Cat No. 31232), sodium citrate dihydrate ( $\geq 99\%$ , FG, Cat No. W302600), FluoroTag™ Fluorescein isothiocyanate (FITC) conjugation kit (Cat No. FITC1), N-(3-Dimethylaminopropyl)-N'-ethylcarbodiimide hydrochloride (EDC hydrochloride,  $\geq 99.0\%$  (AT), Cat No. 03449), 2-(N-Morpholino) ethanesulfonic acid (MES salt, low moisture content,  $\geq 99\%$  (titration), Cat No. M3671), N-Hydroxysuccinimide (NHS, purum,  $\geq 97.0\%$  (T), Cat No. 56480), methacholine chloride (Mch,  $\geq 98\%$  (TLC), powder, Cat No. A2251) and Serelaxin (H2-relaxin, recombinant, expressed in *E. coli*,  $\geq 98\%$  (SDS-PAGE),  $\geq 98\%$  (HPLC), suitable for cell culture, Cat No. SRP3147) were purchased from Merck/Sigma Aldrich (St Louis, MO, USA).

### **Animals**

Female BALB/c mice (7-8 weeks old; provided by Monash University Animal services, Monash University, Clayton, Victoria, Australia) were allowed to acclimatize for at least 4-5 days prior to experimental models of ALI and AAD. Female Balb/c wild type were used as these mice are more prone to a Th2 response and undergo higher allergen specific airway reactivity compared with their male counterparts<sup>22</sup> and other commonly used strains of mice. Mice were housed under a controlled environment on a 12-h light/12-h dark cycle with free access to water and lab chow (Barastock Stockfeeds, Pakenham, Victoria, Australia). All animal experiments described below were approved by Monash University's Animal Ethics Committee (MARF/2019/20917), which adheres to the Guidelines for the Care and Use of Laboratory Animals for Scientific Purposes

(National Health and Medical Research Council of Australia, Canberra, Australia). Power calculations was used to determine group sizes to be 80% powered to detect a 15-25% effect.

### **Fabrication and characterisation of serelaxin-conjugated SPIONs**

Super-paramagnetic iron oxide nanoparticles (SPIONs) were fabricated using a modified alkaline co-precipitation procedure with carboxyl group modified surface, as we have used previously<sup>19,23</sup>. The conjugation of serelaxin (RLX) was performed using carbodiimide chemistry involving N-(3-Dimethylaminopropyl)-N'-ethylcarbodiimide hydrochloride (EDC) and N-Hydroxysuccinimide (NHS)- EDC/NHS reaction. Briefly, 300µl of carboxyl coated SPIONs were added with 2-(N-Morpholino) ethanesulfonic acid (MES buffer, 50mM), NHS buffer (50mM), EDC (4mg/ml) to a final volume of 500µl (pH 5.5-6.5). This conjugation mixture was incubated for 1 hour at room temperature on a rotary wheel. After incubation, the conjugation mixture was purified using a desalting column with 2 repeated washes of 2ml MES buffer (50mM, pH6.0) and centrifuging at 1000g for 2 minutes to remove excess EDC and NHS. RLX Hi (0.05mg/ml) and RLX Lo (0.01mg/ml) was added to the activated SPIONs and incubated overnight at 4°C. The next day, SPIONs conjugated with RLX (NP-RLX) were washed with PBS through a 30 kDa Amicon column and the remaining unconjugated groups were deactivated by glycine (0.1mg/ml) by incubating at room temperature for 30 minutes. The samples were stored at 4°C for further use until experimentation. Fluorescein isothiocyanate (FITC) was conjugated to lysine residues on RLX using the method of Masliah and colleagues<sup>24</sup> and RLX was quantified by ELISA (9.5ng/ml; refer to Supplementary Table 1, Figure 1).

RLX-conjugated SPIONs were characterized for their size, morphology, hydrodynamic size, charge, stability and validation of the conjugation of RLX to the SPIONs. The size and structure

of the particles was measured using a Quantax analysis system and imaged using a FEI Tecnai G2 F20 S-TWIN Field Emission Gun Transmission Electron Microscope (FEGTEM) connected to a wide-angle Orius SCD200 CCD camera. The physicochemical properties of the SPIONs, such as their size, morphology and degree of crystallinity was evaluated by the electron diffraction pattern generated from high resolution transmission electron microscopy (HRTEM). To determine the chemical bonding for conjugating RLX to the nanoparticles, a Fourier-Transformed Infrared Radiation (FTIR) spectrophotometer with a pointed probe was used. The hydrodynamic size was measured using a Malvern Nano-Zetasizer along with the poly-dispersity index (pDI) for stability of the NP-RLX. The charge of the particles was measured using a dip-cell with electrodes, and the number of RLX molecules that were conjugated to each nanoparticle was determined using carbon hydrogen and nitrogen (CHN) analysis<sup>19</sup>. Additional characterisation of the particles was carried out as previously described<sup>23</sup>.

### **Uptake of NP-RLX by immune cells in the lung**

The uptake of NP-RLX by lung immune cells was determined in 8-week old female Balb/c (N=6/group), administered 0.9% saline or 5µg/ml lipopolysaccharide (LPS from *E. coli* K12, Invivogen, San Diego, CA) intranasally on day 1. This was followed by administration of NP-RLX-FITC (200 µg/ml i.n.) to both groups of mice on day 2. On day 4 (48 hours later), mice were culled and the BALF was collected using three repeated washes (of 0.9% saline+10mM EDTA) (see Supplementary Figure 2B). The collected cells were then spotted on a glass slide and stained with DAPI for fluorescence imaging. To identify the location of the nanoparticles within the cells, the cytospot slides were stained with Perl's Prussian blue and counter-stained with neutral red and the cell types were confirmed by staining with Diff Quik for each mouse BALF cytospots.



### **Flow cytometry of NP-RLX uptake**

Based on the uptake observed previously (see section on pulmonary uptake of NP-RLX), we performed flow cytometry on another set of BALF cells (from N=6 mice) following LPS treatment, followed by intranasal NP-RLX-FITC administration (24 hours later; see Supplementary Figure 1B). Another set of mice (N=3) were also treated with NP-RLX, but without the FITC tag to serve as a Fluorescent-Minus-One (FMO) control. BALF cells were treated with ACK lysis buffer followed by resuspension of the cells in FACS buffer (dPBS+5% FCS+0.5mM EDTA). Cells were counted and stained with different antibodies at ( $1 \times 10^5$  cells/ml) in a 50 $\mu$ l volume. The cells were first incubated with a Rat anti-mouse Fc block (CD16/CD32; 553141, 1:50 dilution; BD Horizon, Franklin Lakes, NJ) to prevent non-specific Fc binding. Cell were then stained with CD45-PE-Cy5 (553082, 1:200 dilution; BD Biosciences, San Jose, CA), CD11c-BUV395 (564080, 1:50 dilution; BD Horizon), CD206-AF647 (141711, 1:100 dilution; BioLegend, San Diego, CA), CD68-AF700 (MCA1957A700, 1:100 dilution; Bio-Rad, Berkeley, CA) or F4/80-APC/Fire750 (123151, 1:100 dilution; BioLegend) in FACS buffer. One FMO was stained with all the above-mentioned antibodies to the mice that were not administered the FITC-tagged NP-RLX. The same BALF cells were used for unstained controls. After the primary stain, cells were washed with FACS buffer and resuspended in FACS buffer for secondary staining. For live/dead screening, zombie aqua dye (423101, 1:1000 dilution; BioLegend) in FACS buffer was added to all cells except FMO and unstained controls. The cells were then washed and fixed with dPBS+1% PFA. Cells were acquired on BD Fortessa X20 in Monash Flowcore Platform. The same antibodies were used to prepare compensation beads for single cell controls.

Unstained cells were used to set the voltages for Forward Scatter (FSC) and Side Scatter (SSC), followed by acquiring the single cell control (compensation beads) to perform

compensation controls. Data was analyzed using Flow Jo and statistical calculations performed in GraphPad Prism. Cells were gated on the basis of FSC-A and SSC-A followed by FSC-A and FSC-H for doublet discrimination, and then live/dead screening followed by gating CD45<sup>+</sup> cells for monocytes/macrophages. Cells were further characterized on the basis of the markers used for staining with NP-RLX on the FITC channel and used to determine its uptake. The unstained and FMO controls were used to gate the actual uptake of NP-RLX-FITC by differentiating them from false-positives.

### **Induction and treatment of chronic AAD incorporating airway inflammation, airway remodeling and airway hyperreactivity**

The effects of NP-RLX in a model of chronic AAD were assessed in 7-8-week old female Balb/c mice (N=8/group) sensitized with two i.p injections of 10 µg grade V chicken egg ovalbumin (OVA, Sigma-Aldrich, St-Louis, MO, USA) and 1 mg alum as adjuvant (AJAX Chemicals, Kotara, NSW, Australia) in 0.5ml of 0.9% saline on Days 0 and 14. The mice were then challenged by nebulizing 2.5% (w/v) OVA for 30 mins a day, three times a week, between days 21 to 63, using an ultrasonic nebulizer (Omron NEU07; Omron, Kyoto, Japan). At day 63, these mice present with significant AI, AWR, airway/lung fibrosis and AHR<sup>15</sup>. A control group of mice (N=8) were injected with 0.9% saline i.p. on days 0 and 14; and nebulised with saline only from days 21-63.

On day 64, sub-groups of OVA sensitized and challenged mice were treated with either systemically-infused RLX (0.5mg/kg/day s.c.; a dose that has previously shown therapeutic efficacy in the same murine chronic AAD model<sup>14</sup>) administered using osmotic mini-pumps (Model 1007D, Alzet, Cupertino, CA, USA; which continuously infused RLX into the circulation

at a rate of 0.5 $\mu$ l/hour over a 7 day period); or NP-RLX Hi (25ng/ml), NP-RLX Lo (5ng/ml) or NP-empty (without RLX), administered intranasally every 48 hours (thrice during the 7 day treatment period) from days 64 to 70 (see Supplementary Figure 2C). Mice were subjected to invasive plethysmography on day 71 to measure airway/lung function, before being culled for evaluation of BALF and tissue end-points.

### **Invasive plethysmography**

On day 71 of the chronic AAD model (24 hours after the 7-day treatment period), mice were subjected to invasive plethysmography to evaluate AHR and dynamic lung compliance, in response to increasing nebulised concentrations of methacholine (0-50mg/ml). Mice were briefly anaesthetised with ketamine (100mg/kg body weight, i.p.) and xylazine (20mg/kg body weight, i.p.), tracheostomized and cannulated. Airway resistance was measured in a Buxco Rodent RC site (Biosystem XA xersion 2.7.9, Buxco Electronics, Troy, NY, USA) for 3 min after each dose. Dynamic lung compliance was also evaluated for each dose of methacholine and both resistance and compliance expressed as the percentage change from baseline<sup>25</sup>.

### **Tissue collection, histopathology and immunohistochemistry**

BALF was collected after lung function measurements, while animals were still anaesthetised, whereby the lungs were washed three times with 0.9% saline. Mice were then culled with an overdose of anaesthetic (10:1 mixture of ketamine and xylazine, each at 100mg/ml), followed by cervical dislocation. The lung tissue was then isolated, weighed and separated into individual lobes. The largest lung lobe was fixed in 10% neutral-buffered formalin (NBF) overnight and

processed to be cut and embedded in paraffin wax; and the remaining lobes were individually snap-frozen in liquid nitrogen and stored at -80°C until required.

Serial paraffin-embedded lung sections (4µm thickness) were placed on charged SuperFrost glass slides (Grate Scientific, Ringwood, Victoria, Australia). Serial sections from each lung were stained with Mayer's hematoxylin and eosin (H&E), Masson's trichrome or Alcian blue periodic acid Schiff (ABPAS) for assessment for airway/lung inflammation, epithelial thickness and subepithelial collagen deposition, and goblet cell metaplasia, respectively<sup>14</sup>. Additional serial sections were immunohistochemically-stained using polyclonal antibodies for CD206 (a marker of M2 macrophages; 141711, 1:500 dilution; BioLegend, San Diego, CA); iNOS (a marker of M1 macrophages; 13120S, 1:100 dilution; Cell Signaling Technology, Danvers, Massachusetts, USA); airway/lung thymic stromal lymphopoietin (TSLP; a marker of epithelial damage; ABT330, 1:5000 dilution; EMD Millipore Corp'. Temecula, CA, USA), TGF-β1 (GTX110630, 1:1000; GeneTex, Irvine, CA, USA); α-smooth muscle actin (a marker of myofibroblast differentiation; ab5694, 1:1000; Abcam, Cambridge, MA, USA); and the pro-inflammatory cytokines: IL-1β (bs-0812R, 1:1500; Bioss antibodies, Boston, MA), IL-6 (E-AB-40021, 1:2000; Elabscience, Houston, TX) or TNF-α (ab6671, 1:250; Abcam). Similarly, phosphorylated Smad2 (pSmad2, an intracellular protein that promotes TGF-β1 signal transduction/activity was stained with a rabbit monoclonal antibody; 3108, 1:250; Cell Signaling Technology). The primary antibodies were detected using the DAKO EnVision anti- anti-rabbit kit (K4003, DAKO, Glostrup, Denmark) along with 3,3-diaminobenzidine (DAB, Sigma-Aldrich, Richmond, CA), where sections were counter-stained with haematoxylin. All slides were then scanned at the maximum magnification available (40x) using Leica Biosystems microscope connected with a ScanScope AT Turbo (Aperio, CA, USA).

### **Morphometric analysis**

Digitally-scanned slides were viewed and morphometrically analyzed in a blinded fashion, with Aperio Image scope v12.4.3 software (Leica Biosystems, Nussloch, Germany). Morphometric analysis was performed on five randomly-selected airways from across the tissue sample and histologically graded for inflammation severity as described previously<sup>25</sup>. Masson's trichrome stained slides were analyzed by measuring the thickness of the epithelium and sub-epithelial layers, and expressing the values as  $\mu\text{m}^2$  mm basement membrane (BM) length as we described previously<sup>15,25</sup>. ABPAS-stained slides were analyzed by counting the number of goblet cells (purple) expressed as  $\mu\text{m}^2$  or  $\mu\text{m}$  per 100 $\mu\text{m}$  BM length. TSLP and pSmad2 positive cells detected within the epithelium of the airway were counted and expressed as number of positively-stained cells per 100 $\mu\text{m}$  BM length. The  $\alpha$ -smooth muscle actin positively stained cells were located within the subepithelial or interstitial regions and expressed per 100 $\mu\text{m}$  BM length. TGF- $\beta$ 1 staining was quantified by evaluating the levels of strong positive stained areas within the epithelial and interstitial regions and expressing the data as epithelial TGF- $\beta$ 1 staining per field (%). Likewise, pro-inflammatory cytokines were quantified for each section/animal where several sections were identified and scored subtracting the background<sup>26</sup>. The total intensity of the strong positive stained area for each section/mouse was recorded using the Aperio Imagescope positive pixel count algorithm<sup>25,26</sup>.

### **ELISA analysis**

The BALF supernatants of saline, OVA and OVA-treated mice was used to detect the levels of CCL2/MCP-1 (DY479, Mouse CCL2 DuoSet ELISA kit, R&D Systems, Minneapolis, MN, USA)

and CCL11/eotaxin-1 (DY420, Mouse CCL11 DuoSet ELISA kit, R&D Systems, Minneapolis, MN, USA), as chemokines involved in macrophage and eosinophil recruitment to sites of injury, respectively. The H2 relaxin ELISA (DRL200, Human Relaxin-2 Quantikine ELISA kit, R&D Systems, Minneapolis, MN, USA) was used to determine the efficacy and bioavailability of circulating relaxin in the sera of OVA sensitized and challenged mice treated with either Pump-RLX, NP-RLX Hi, NP-RLX Lo or NP-empty. In all cases, analyses were performed according to the manufacturers' instructions.

### **Cytospot and differential cell count**

Cells collected from BALF were spotted on glass slides with prior treatment of ACK (Ammonium-Chloride-Potassium) red cell lysis buffer. The spotted cells were stained with Diff Quik to perform differential cell counts for immune cells based on the nuclear morphology of the cells, as previously described<sup>14</sup>.

### **Culture of primary airway fibroblasts**

Non-asthmatic and asthmatic primary airway (myo)fibroblasts were generated from normal bronchial tissue, collected from 3 non-asthmatic and 3 asthmatic subjects after lobectomy for operable lung cancer. Primary cells were kindly provided by Prof. Phillip Bardin and Dr. Belinda Thomas (Hudson Institute of Medical Research, AU). Cells were maintained at 37°C in 5% CO<sub>2</sub> air in Minimum Essential Media (MEM, for primary lung fibroblasts) (supplemented with 2 mM in L-glutamine, 10% v/v fetal bovine serum (FBS) and 100 U/mL penicillin G). Cells were split at a 1:4 ratio per week and grown to confluence for use between passages 4-6 for PF. Flasks of cells which were <70% viable were not used for experiments.

### **Preparation of Collagen Gels**

Rat tail tendon collagen was prepared as we previously described<sup>27</sup>. Briefly, collagen bundles from rat tails were dissected under aseptic conditions and extracted in 0.5M acetic acid at 4°C and allowed to cool for 24 hours. This solution was centrifuged at 10,000rpm at 4°C for 2 hours over 3 days to separate the collagen solution from the collagen fibres (fibrillar type I collagen). The collagen solution was dialysed in water to remove any excess acetic acid and stored at 20°C.

Confluent (myo)fibroblasts were serum-deprived for 72 hours in FBS-free media to stop cell growth. Cells were trypsinised and resuspended at  $0.5 \times 10^6$  cells/mL in 4X DMEM and combined with the collagen solution (1-part cells:3-part collagen) at 4°C. The cell-collagen mixture was transferred into 24-well culture plates (500  $\mu$ L/gel). Once set, gels were dislodged into 6-well culture plates with 1 mL 1xMEM and suspended in a total volume of 3 mL 1X MEM at 37°C for up to 48 hours.

### **Collagen Gel Experiments**

Gels were treated at t=0 with TGF- $\beta$ 1 (2ng/mL) in the absence and presence of RLX (10ng/mL), NP-RLX Hi, NP-RLX Lo or left untreated apart from the addition of vehicles (NP-empty, 20 mM sodium acetate buffer). Images were captured at t=0, 1, 2, 4, 24, 48 and 72 hours.

Initial gel areas were constrained to the diameter of a single well within a 24-well plate. Areas of gels at all time points were manually measured with Image J and expressed as % of well area in a 6-well plate. This was then normalised to gel area at t=0 and expressed as gel contraction (% initial area).

## **Data and statistical analysis**

Experimental data demonstrated for nanoparticle characterization based on 8 successive replicates and three representative datasets are presented in the figures. All data are expressed as the mean  $\pm$  standard deviation (SD) and all statistical analyses was performed using GraphPad Prism v8.0 (GraphPad Software Inc., CA, USA). Lung function data was assessed by a two-way ANOVA with Bonferroni's *post hoc* test. A Mann-Whitney U-test was used to compare differences between non-parametric groups. All other data was assessed using a one-way ANOVA with Tukey's *post hoc* test for multiple comparisons between the groups. In each case, significance was classified as being  $P < 0.05$ .



## Results

### Characterisation of RLX-conjugated SPIONs (NP-RLX)

To develop a sustainable and translatable therapy for asthma, we conjugated serelaxin (RLX) to super-paramagnetic iron oxide nanoparticles (SPIONs). For this purpose, we functionalised pristine SPIONs with carboxylic acid groups (COOH)<sup>23</sup>, and conjugated them with RLX (NP-RLX) using carbodiimide chemistry (Figure 1A). The purified NP-RLX was physiochemically characterized for its size, hydrodynamic size and charge. The conjugation of RLX to SPIONs was validated using Fourier-transform infrared spectroscopy (FTIR)<sup>26</sup>, and using the H2 RLX Quantikine<sup>®</sup> ELISA. NP-RLX was imaged using high resolution-transmission electron microscopy (HR-TEM)<sup>23,26</sup>, for nanoparticle core size ( $6.9\pm 3.2\text{nm}$ , shown in brown), while RLX (shown in green) was present as a corona (Figure 1B) and was found to be crystalline with the selected area electron diffraction pattern consistent for SPIONs (Figure 1B-inset)<sup>23</sup>. The successful conjugation of RLX to SPIONs was confirmed by a red shift of the RLX peaks at 1711 (C=O stretching), 1400 (C-N stretching) and 1278/cm (O-H bending) to 1617, 1193 and 1045/cm, respectively (Figure 1C). The signature peaks for SPIONs without RLX but with the conjugation arm (SPION-Carbodiimide-N-Hydroxysuccinimide) at 2988, 2902, 1412, 1248 and 1062/cm, was absent after RLX conjugation, signifying the successful bonding of RLX. Dynamic light scattering (DLS) showed an increase in hydrodynamic size ( $75.57\pm 4.2\text{nm}$ ) and had good colloidal stability (poly-dispersity index, PDI: 0.155) (Figure 1D). Furthermore, negative surface charges ( $\zeta$ , zeta-potential) increased to  $-47.3\pm 12.2\text{mV}$  (Figure 1E), indicating successful RLX conjugation. Using CHN analysis, it was determined that 19,380 RLX molecules were attached to each particle. We then determined using the H2 RLX Quantikine<sup>®</sup> ELISA that 10,500ng and 3,500ng of RLX was

conjugated to SPIONs when 25 $\mu$ g (0.05mg/ml) and 5 $\mu$ g (0.01mg/ml) of RLX was used (data shown in Supplementary Table 1; Supplementary Figure 1).

NP-RLX preparations were then used at two doses, NP-RLX (Hi)gh (25ng/ml) which was consistent within the range of circulating RLX found 5-14 days after systemic RLX (0.5mg/kg/day)-treatment of mice (via osmotic minipump<sup>28</sup>); or NP-RLX Lo(w) (5ng/ml) for subsequent studies in murine models of acute lung injury (ALI)<sup>29</sup> and chronic AAD. For investigations delineating the role of RLX in altering lung macrophage populations, NP-RLX was conjugated with fluorescein isothiocyanate (FITC), to Lys17 residue (A chain) and Lys33 residue (B chain), with a fluorescent dye to protein ratio of 0.73 $\pm$ 0.08 (refer Supplementary Figure 2).

#### **NP-RLX uptake by alveolar macrophages is enhanced under inflammatory conditions.**

The uptake of NP-RLX by inflammatory cells was evaluated in an ALI model<sup>29</sup>, whereby mice were administered either saline (vehicle control) or lipopolysaccharide (LPS; 5 $\mu$ g/ml; i.n.), followed by FITC-labelled NP-RLX administration (10 $\mu$ g particles per mouse; i.n; equivalent to 25ng/ml RLX) after 24 hours (Supplementary Figure 2B). Model validity was confirmed by the influx of neutrophils and alveolar macrophages as evident by Diff-Quik staining (Figure 2A). FITC-tagged NP-RLX was localised to the cytoplasm of alveolar macrophages but was absent from the nucleus, as evident from Prussian blue staining for the SPION core (Figure 2B, 2C). In cytopots of bronchoalveolar lavage fluid (BALF) collected 48 hours after LPS exposure and stained with nuclear stain DAPI, NP-RLX was preferentially taken up by alveolar macrophages in the inflamed airways of LPS-treated mice (Figure 2C; Supplementary 3), despite the high number of neutrophils also present in the BALF (Figure 2A). Alveolar macrophages were increased in size by LPS exposure (Figure 2D). When normalised for cell area, alveolar macrophages in LPS-treated mice had taken up 33% more NP-RLX compared to their counterparts from saline-treated (vehicle

control) mice (Figures 2E). On the other hand, NP-empty appeared to be preferentially taken-up by neutrophils, both in the lung tissue (Supplementary 3A) as well as BALF (Supplementary 3B) and were degraded in the liver (Supplementary 3C).

### **Infiltrating CD206<sup>+</sup> and tissue-resident CD68<sup>+</sup> macrophages are selectively involved in the uptake of NP-RLX.**

To identify macrophage subsets that were taking up NP-RLX in the airways, FACS of viable cells from the BALF of LPS-inflamed/NP-RLX-treated mice was conducted (Figure 3A). We identified monocytes/macrophages by gating for CD45<sup>+</sup> cells. The mannose receptor (CD206) expressed on the surface of alternatively activated (M2) macrophages was used to differentiate the population of cells based on their inflammatory phenotypes: M1 (F4/80<sup>pos</sup>CD206<sup>neg</sup>) and M2 (F4/80<sup>pos</sup>CD206<sup>pos</sup>). M2 macrophages demonstrated a 3.5-fold higher uptake of NP-RLX compared to M1 macrophages (Figure 3B); and based on CD11c<sup>pos</sup> myeloid cells within the subsets CD206<sup>pos</sup> and CD206<sup>neg</sup> macrophages, the uptake of NP-RLX was found only on CD206<sup>pos</sup> cells (Figure 3C). Similarly, the presence of CD206 was associated with the uptake of NP-RLX by CD68<sup>pos</sup> monocytes/macrophages (Figure 3D). Two different populations of CD11c<sup>pos</sup> cells: CD11c<sup>lo</sup> and CD11c<sup>hi</sup> were identified; where a higher uptake of NP-RLX was proportional to higher expression of CD11c and negligible for CD11c<sup>lo</sup> (Figure 3E).

Three lung macrophage subpopulations including interstitial macrophages were further identified based on CD68 expression: CD68-negative (CD68<sup>neg</sup>), CD68-low (CD68<sup>lo</sup>), and CD68-high (CD68<sup>hi</sup>) (Figure 4A). Of the total BALF cell population, CD68<sup>hi</sup> (7%) and CD68<sup>lo</sup> (19%) cells had higher uptake of NP-RLX than CD68<sup>neg</sup> cells (~73%). Subsets of CD68<sup>hi</sup> were then further evaluated based on F4/80 and CD11c (Figure 4B, 4C). A subset of lung dendritic cells was characterized as CD11c<sup>pos</sup>F4/80<sup>neg</sup> cells (Figure 4B) having lower NP-RLX uptake than F4/80<sup>pos</sup>

macrophages. A majority of CD68<sup>hi</sup> monocytes/macrophages obtained from single cell suspensions were found positive for CD11c and F4/80 (Figure 4B). Based on our findings and studies by others<sup>30</sup>, we identified alveolar macrophages as CD68<sup>hi</sup>/F4/80<sup>pos</sup>/CD11c<sup>pos</sup> cells. These cells demonstrated the highest uptake of NP-RLX, ~8-fold higher than by CD68<sup>hi</sup>/F4/80<sup>pos</sup>/CD11c<sup>neg</sup> cells. By further investigating CD68<sup>hi</sup> cells in the BALF, a population of CD68<sup>hi</sup>/CD11c<sup>pos</sup> leukocytes, that were negative for F4/80, was detected. NP-RLX uptake by these cells was less than that taken up by F4/80<sup>pos</sup> cells, but higher than that taken up by CD68<sup>hi</sup>/F4/80<sup>pos</sup>/CD11c<sup>neg</sup> cells (Figure 4B). In contrast, cells which were double negative for CD11c and F4/80 demonstrated negligible uptake of NP-RLX.

CD68 is found in immigrant monocytes, hence their lower expression is associated with interstitial macrophages within the lung; and NP-RLX uptake by CD68<sup>lo</sup> cells was also evaluated. From the CD68<sup>lo</sup> (and CD68<sup>neg</sup>) leukocyte gates, we found that autofluorescence in each additional channel (including those used for CD11c and F4/80 staining) was lower in comparison to the negative control from the CD68<sup>hi</sup> compartment (Figure 4C). Based on this strategy, we found that approximately 19% of cells in the CD68<sup>lo</sup> gate were positive for F4/80, and ~27% were positive for CD11c. In the CD68<sup>lo</sup>/CD11c<sup>pos</sup> population, the uptake of NP-RLX was significantly higher in F4/80<sup>pos</sup> cells compared to F4/80<sup>neg</sup> cells (Figure 4C). In another population of CD11c<sup>neg</sup>/F4/80<sup>pos</sup> cells there was negligible NP-RLX uptake.

### **NP-RLX reduces established airway inflammation in mice with chronic AAD**

Mice were sensitized and challenged with ovalbumin (OVA) or saline (vehicle) over a 9-week period. At this time-point, OVA-challenged mice had an abundance of CD206<sup>+</sup> M2 macrophages but very little iNOS<sup>+</sup> M1 macrophages in their airways (see Supplementary Figure 4), which indicated that there was already a large number of M2 macrophages to uptake NP-RLX. OVA-

challenged mice were then either left untreated for a further 1-week (OVA mice) or treated with systemically-delivered RLX (Pump-RLX; 0.5mg/kg/day for 7 days; which produced circulating levels of ~18ng/ml after 7 days of administration (see Supplementary Figure 5) or with NP-RLX Hi (25ng/ml; which produced circulating levels of ~22ng/ml; Supplementary Figure 5), NP-RLX Lo (5ng/ml; which produced circulating levels of ~4ng/ml; Supplementary Figure 5) or NP-empty (nanoparticles without RLX), given intranasally at 48 hr intervals (Supplementary Figure 2C).

OVA alone induced an increase in peribronchial AI (by ~5.5-fold median increase; Figures 5A, B), pro-inflammatory cell influx within the BALF (Figure 5C-G), and mucin-producing goblet cell metaplasia (by ~13-fold; Figures 5H, 5I), compared to saline-treated control mice. Consistent with the human allergic asthma phenotype, OVA-challenged mice had significantly increased total BALF inflammatory cell counts (Figure 5C), as well as markedly higher numbers of eosinophils (Figure 5D) and macrophages (Figure 5E), compared to their saline sensitized and challenged counterparts. There were smaller OVA-induced increases in other inflammatory cells such as neutrophils (Figure 5E) and lymphocytes (Figure 5F). These OVA-induced features represented those frequently found in human asthma sufferers with chronic disease symptoms<sup>31,32</sup>.

Pump-RLX and NP-RLX Hi equivalently reduced the OVA-induced increase in peribronchial AI (by ~58-60%; Figure 5B); and equivalently ameliorated BALF total cell counts (by ~42-47%; Figure 5C), eosinophils (by ~55-67%; Figure 5D), macrophages (by ~38-51%; Figure 5E) and goblet cell metaplasia (by ~83-87%; Figure 5H, 5I). In most cases, this was to a greater extent than NP-RLX Lo treatment of mice, which only reduced the OVA-induced peribronchial AI (Figure 5B), eosinophils (Figure 5D), macrophages (Figure 5G) and goblet cell metaplasia (Figure 5I) by ~19-37%. For all outcomes, this was to a greater extent than NP-empty treatment of mice, which did not significantly affect the OVA-induced inflammatory measures. The anti-inflammatory

effects of NP-RLX were more pronounced on BALF eosinophils and macrophages, compared to other immune cells evaluated; with neither Pump-RLX or NP-RLX at either dose affecting the OVA-induced increase in neutrophils (Figure 5E) or lymphocytes (Figure 5F). Furthermore, the OVA-induced increase in airway/lung oedema (Figure 5A) appeared to be unaffected by NP-empty treatment, partially reduced by Pump-RLX or NP-RLX Lo treatment, and fully reduced with NP-RLX Hi treatment after 7 days. The anti-inflammatory effects of NP-RLX were dose-dependent with more pronounced effects induced by NP-RLX Hi compared to NP-RLX Lo treatment.

### **NP-RLX reduces pro-inflammatory cytokine expression in mice with chronic AAD**

To examine the effects of OVA treatment on the gene expression of inflammatory and remodelling markers, analysis was performed on datasets from the Gene-Expression Omnibus database for whole lung tissue from saline- vs OVA-sensitized and challenged mice (GSE41667, Figure 6A) and more specifically, alveolar macrophages (GSE79592<sup>33</sup>, Figure 6B). RLX treatment had previously been shown to attenuate cardiac fibrosis by modulating TGF- $\beta$ 1-induced interstitial and ventricular collagen deposition<sup>34</sup>. Furthermore, to investigate the involvement of TGF- $\beta$ 1 and its associated pro-inflammatory effects, the data obtained from the murine lung and lung macrophages was compared to reanalysis of the inflammatory and tissue remodelling marker gene expression from the inflamed hearts of aged (2-year old) rats as well as the hearts of RLX-treated rats, using the Gene Expression Omnibus dataset (GSE106337<sup>35</sup>, Figure 6C).

Noticeably, the pro-inflammatory cytokines *Il-1 $\beta$* , *Il-6*, *TNF- $\alpha$*  and *TGF- $\beta$ 1*, the epithelial injury marker *TSLP* and fibrotic markers *pSmad2* and  *$\alpha$ -SMA* were significantly upregulated in both GSE41667 and GSE79592<sup>33</sup> datasets (Figures 6A, 6B). Additionally, gene expression of the chemokines *Ccl2* and *Ccl11*, which are responsible for alveolar macrophage and eosinophil influx,

were significantly upregulated in both datasets. Consistent with these changes, the gene expression of *Il-1 $\beta$* , *Il-6*, *TNF*, *TGF- $\beta$ 1*, *pSmad2* and  *$\alpha$ -SMA* were all upregulated in the inflamed heart of aged rats, but were down-regulated by Pump-RLX treatment<sup>35</sup> (Figure 6C), consistent with our findings in the OVA-induced chronic AAD model.

Immunohistochemistry of inflammatory cytokines in lung tissue sections confirmed that OVA-sensitized and challenged mice had significantly increased IL-1 $\beta$  (Figure 6D), IL-6 (Figure 6E) and TNF- $\alpha$  (Figure 6F) expression (by ~6-9-fold) in the lung parenchyma and specifically around the airways (Supplementary Figure 6), compared to saline-treated controls. This OVA-induced increase in IL-1 $\beta$  (by ~90-95%; Figure 6D) and IL-6 (by ~77-90%; Figure 6E) expression was markedly and equivalently reduced by Pump-RLX or NP-RLX Hi treatment after 7 days; whereas Pump-RLX (by ~90%) had a greater effect in reducing the OVA-induced increase in lung TNF- $\alpha$  expression compared to NP-RLX Hi treatment (which only reduced it by ~67%; Figure 6F). In comparison, NP-RLX Lo treatment more modestly reduced only the OVA-induced IL-6 and TNF- $\alpha$  (by ~25-30%); whereas the OVA-induced increase in all three pro-inflammatory cytokines was unaffected by NP-empty treatment.

ELISA analysis of BALF chemokines that are involved in the recruitment of macrophages (CCL2/MCP-1; Figure 6G) or eosinophils (CCL11; Figure 6H) were also measured. OVA-sensitized and challenged mice were found to have significantly increased BALF levels of CCL2 (by ~27-fold) and CCL11 (by ~9-fold) compared to corresponding chemokines levels measured in the BALF of saline sensitized and challenged mice; which would be expected to facilitate the increased recruitment of macrophages and eosinophils to the inflamed airways/lungs of OVA-injured mice. While this OVA-induced increase in CCL2 (Figure 6G) and CCL11 (Figure 6H) were equivalently reduced by Pump-RLX or NP-RLX Hi (by ~60-75%), and to a lesser extent by

NP-RLX Lo (by ~31-33%), the abundance of resident M2 macrophages in the airways of OVA sensitized and challenged mice (Supplementary Figure 4) and capacity of macrophages to undergo phagocytosis likely explains why NP-RLX was taken up by M2 macrophages. In comparison, the lower number of eosinophils and inability of eosinophils to undergo phagocytosis is consistent with the lack of uptake of NP-RLX by this subtype of leukocytes. In both cases, NP-empty treatment of OVA-injured mice did not significantly affect the OVA-induced increase in CCL2 (Figure 6G) or CCL11 (Figure 6H) levels.

### **NP-RLX reduces established AWR including airway fibrosis in mice with chronic AAD**

OVA-injured mice also underwent significantly increased airway epithelial thickness (by ~1-fold; Figures 7A, 7B), subepithelial thickness (by ~3-fold; Figure 7C) and thymic stromal lymphopietin (TSLP)-associated epithelial damage (by ~3.5-fold; Supplementary Figure 7; Figure 7D), compared to respective measurements obtained from saline-treated mice. NP-RLX Hi treatment abrogated the OVA-induced increase in airway epithelial thickening, to a greater extent than Pump-RLX treatment (which reduced airway epithelial thickening by ~70%; Figure 7B); but equivalently reduced the OVA-induced increase in subepithelial ECM thickness (by 73-77%; Figure 7C) and TSLP-associated epithelial damage (by ~55-60%; Figure 7D), to a similar extent as Pump-RLX treatment. In comparison, NP-RLX Lo treatment of OVA-injured mice modestly reduced almost all these measures of AWR and epithelial damage (by ~10-25%; Figures 7A-D).

Furthermore, OVA-injured mice also presented with significantly increased epithelial TGF- $\beta$ 1 expression (by ~30-fold; Supplementary Figure 7; Figure 7E); Smad2 phosphorylation (pSmad2; by ~3.7-fold; Supplementary Figure 7; Figure 7F); and subepithelial myofibroblast accumulation (by ~8.8-fold; Supplementary Figure 8; Figure 7G) compared to respective measurements obtained from saline-treated mice. NP-RLX Hi treatment of OVA-injured mice



abrogated airway epithelial thickening, to a greater extent than Pump-RLX treatment (which reduced airway epithelial thickening by ~70%; Figure 7B); equivalently reduced the OVA-induced increase in subepithelial ECM thickness (by 73-77%; Figure 7C), TSLP-associated epithelial damage (by ~55-60%; Figure 7D), epithelial TGF- $\beta$ 1 expression (by 60-65%; Figure 7E) and pSmad2 (by ~50-65%; Figure 7F) to a similar extent as Pump-RLX treatment; but reduced subepithelial myofibroblast accumulation (by ~25%), to a lower extent than Pump-RLX treatment (which reduced subepithelial myofibroblast accumulation by ~51%; Figure 7G). In comparison, NP-RLX Lo treatment of OVA-injured mice modestly reduced airway/lung fibrosis (by ~10-35%; Figures 7E-G), without significantly affecting subepithelial myofibroblast accumulation (Figure 7G). NP-empty treatment of OVA-injured mice did not affect any feature of AWR/fibrosis, suggesting that SPIONs alone did not induce anti-AWR effects. There was also a noticeable increase in the lung dry weight of OVA-induced AAD mice compared to that measured from saline-treated controls (Supplementary Figure 2A); which is consistent with the aforementioned airway/lung fibrotic changes measured.

### **NP-RLX reduces established AHR and loss of dynamic lung compliance in mice with chronic AAD**

In line with the increased AI, AWR and airway/lung fibrosis measured from OVA-injured mice, these animals had increased AHR (by ~5-fold at the highest dose of methacholine evaluated; Figure 7H) and a loss of dynamic lung compliance (by ~0.55-fold; Figure 7I), compared to respective measurements from saline-treated mice. The OVA-induced AHR was reduced to a similar extent after 7 days of NP-RLX Lo (by ~55%), NP-RLX Hi (by ~75%) and Pump-RLX (by ~70%) treatment, but not fully back to levels measured from saline-treated mice (Figure 7H). The OVA-induced loss of dynamic lung compliance was completely restored by all three RLX-treated

groups (Figure 7I). However, NP-empty treatment of OVA mice did not affect either the OVA-induced AHR or loss of dynamic lung compliance.

### **NP-RLX inhibits TGF- $\beta$ 1-mediated contraction of collagen gels seeded with airway (myo)fibroblasts from patients with or without an asthma diagnosis**

Contraction of (myo)fibroblast-containing collagen gels provides an indication of their pro-fibrotic function and potential to remodel the three-dimensional gel structure by collagen condensation rather than collagen degradation. While cell-mediated reductions in gel area are known to be further increased by TGF- $\beta$ 1<sup>27</sup>, the effects of asthma status, and of RLX vs NP-RLX on this process, have yet to be defined.

In collagen gels seeded with primary human airway fibroblasts, time-dependent reduction in gel area was clearly evident within 24 hours (Figure 8A, B). At cell density (seeding  $0.5 \times 10^6$  cells/ml) matched across all gels at 48 hours, contraction of gels containing non-asthmatic fibroblasts was less than gels containing asthmatic myofibroblasts, with reductions of  $12 \pm 1\%$  and  $29 \pm 9\%$ , respectively (Figure 8A-D). A further increase in cell-mediated contraction was evident within 24 hours of TGF- $\beta$ 1 stimulation, reducing the area of gels seeded with non-asthmatic and asthmatic (myo)fibroblasts by an additional 12% and 34%, respectively, after 48 hours in total (Figure 8A-C); while gels without cells showed no contraction (data not shown).

None of the treatments evaluated prevented gel contraction in the absence of TGF- $\beta$ 1 (data not shown). However, the significant increase in TGF- $\beta$ 1-induced gel contraction was partially inhibited by RLX, NP-RLX Lo and NP-RLX Hi in both non-asthmatic or asthmatic fibroblasts (all NS compared to untreated gels). NP-RLX Hi was more effective than RLX or NP-RLX Lo in reducing the amplified response to TGF- $\beta$ 1 in gels containing myofibroblasts from asthma patients than from non-asthma patients (Figure 8D, 8E).

## Discussion

The findings of this study have demonstrated for the first time, the feasibility and clinical potential of nanoparticle-conjugated (NP)-RLX as a treatment for chronic AAD. Conjugation of RLX to carboxyl-modified biodegradable SPIONs allowed these nanoparticles to serve as a novel vehicle for the cellular uptake and targeted delivery of RLX by both infiltrating and tissue-resident macrophages. In particular, the abundance of M2 macrophages in the inflamed lungs of (LPS- or OVA-treated) mice and the phagocytic capacity of these macrophages allowed for their uptake of NP-RLX. SPIONs can conjugate compounds with molecular weights as high as 170 kDa in size<sup>36</sup>; and can be fluorescently-tagged for monitoring *in vivo*. As a vehicle, SPIONs also protected RLX's functionality and efficacy. Another advantage of using functionalised SPIONs, is that they can attach to proteins (here RLX; which is normally prone to oxidative degradation<sup>37</sup>) without inducing an inflammatory reaction<sup>38</sup>. Of note, the efficacy of RLX was maintained when administered intranasally every 48-hours, overcoming the need for its continuous administration based on its short *in vivo* half-life of ~10-15 minutes<sup>16</sup>. Importantly, three intranasal administrations of NP-RLX Hi (25 ng/ml) over 1-week period produced the same therapeutic efficacy in ameliorating established AI, AWR and AHR, as continuous Pump-RLX treatment; which produced RLX levels that were similar to that measured in women undergoing multiple pregnancies at the one time<sup>39</sup>. NP-RLX also inhibited TGF- $\beta$ 1-stimulated collagen gel contraction by human airway myofibroblasts from patients with asthma to a greater extent than unconjugated RLX *in vitro*.

The hydrodynamic size of SPIONS used (50-100nm) was chosen to maximise their stability in solution as required for pulmonary delivery. Even though these particles increased in size following RLX conjugation, they still retained a size <100nm, that resulted in their uptake by antigen-presenting immune cells<sup>38</sup>. High resolution TEM demonstrated that the conjugated RLX was present on the surface of the nanoparticles. This resulted in an increased negative charge on

the particle surface (owing to the presence of carboxyl groups) from the conjugation of RLX; which was biocompatible for RLX uptake by antigen-presenting cells<sup>38,40</sup>. However, measurement of active RLX levels using ELISA, remained unaffected by the surface charge (Supplementary Table 1). Importantly, similar levels of RLX were measured from NP-RLX made fresh compared to when these particles were stored at 4°C for 6 months, indicating that they could retain the efficacy of RLX several months after conjugation. However, a potential drawback to using these SPIONs is their limited availability of free carboxyl groups on their surface to conjugate RLX (or any other molecule), owing to steric hindrance. Hence, it was found that these SPIONs could only conjugate RLX at concentrations of up to 60ng/ml. Although RLX is known to induce bell-shaped dose-response effects<sup>41,42</sup>, attributed to the differential signaling of G-proteins downstream of its binding to RXFP1<sup>43</sup>, systemic levels of RLX (within ~10-100ng/ml) have been found to induce optimal collagen-inhibitory effects in TGF-β1-stimulated human lung myofibroblasts<sup>41</sup>. In line with this, we confirmed that unconjugated RLX or NP-RLX could equivalently reduce TGF-β1-stimulated collagen I expression levels from human asthmatic lung myofibroblasts at doses of 25ng/ml or 60ng/ml (Supplementary Figure 9). On the other hand, higher levels of RLX (>80-100ng/ml) can lead to receptor de-sensitisation,<sup>17,44</sup> and lower physiological responses.

On the other hand, the use of SPIONs for the pulmonary delivery of RLX had several advantages over other types of nanoparticles available, in terms of their limited toxicity and biodegradability. SPIONs can be retained in biological environments for prolonged periods (up to ~2-3 days) without evoking an immune response and ensuing tissue inflammation. The decoration of the SPION surface with charged proteins/peptides enhances their biocompatibility and prevents their entry with their conjugated peptides/drugs to the cell nucleus<sup>38,45</sup>. Furthermore, SPIONs are detectable using common histochemical staining techniques and prevent mucociliary clearance when delivered into the pulmonary system. Under normal circumstances, the airway epithelium

consists of basal, ciliated and mucus-producing goblet cells that form a highly-regulated and impermeable barrier<sup>46</sup>. In asthma, however, the airway epithelium displays structural abnormalities associated with airway smooth muscle hypertrophy, mucus production and impaired barrier structure, which would underpin dysregulated differentiation and loss of ciliated epithelial cell function<sup>46</sup>. It is plausible that NP-RLX was capable of escaping the disrupted epithelium. In addition, the hydrodynamic size of NPs (<100 nm) would have prevented the expulsion of these ultra-fine particles<sup>47,48</sup>. However, beyond 48-72 hours of administration, NPs are degraded by endosomes and returned to blood as iron before excretion<sup>20</sup>, and hence, were administered every 48 hours at a particle load of 200µg/ml<sup>21,23,38</sup> (over the 1-week treatment period investigated). The biodegradability of SPIONs after 48-72 hours of administration also enabled us to utilise carboxylated SPIONs (NP-empty) as control vehicles, to ensure that the SPIONs themselves were not inducing any adverse or therapeutic effects in the models employed. The release of RLX into the airways/lungs was potentially mediated by a pH-shift within the alveolar macrophages that took up NP-RLX, as studies have shown that macrophages undergo an acidic pH to release compounds conjugated to SPIONs<sup>49,50</sup>. To validate that RLX was able to leave the macrophages, we investigated RLX levels in the sera of OVA challenged mice that were treated with either RLX-pump, NP-RLX or NP-Empty (Supplementary Figure 5). Equivalent levels of circulating RLX levels were measured following Pump-RLX or NP-RLX Hi treatment (~18-22ng/ml), while lower circulating levels of RLX were determined following NP-RLX Lo treatment (~4ng/ml); which indicated that ~80-90% of the conjugated RLX that was originally administered to mice, could be detected in the circulation of treated mice after three administrations, 48 hours apart. This validated that RLX was released from the NPs to induce its therapeutic effects in the model studied.

Interestingly, while NP-RLX appeared to be predominantly taken up by M2 alveolar

macrophages, the uptake of NP-empty appeared to be carried out by neutrophils and were eventually cleared from the liver (Supplementary Figure 3). This cell-selective uptake of NP-RLX may have been influenced by the use of LPS (which is TLR-4 agonist), which is a known promoter of macrophage activation and the production of the pro-inflammatory cytokines, IL-1 $\beta$  and TNF- $\alpha$ <sup>51</sup>, as well as an inhibitor of macrophage phagocytosis of apoptotic neutrophils<sup>52</sup>. Additionally, the increased expression of the chemokines, *Ccl2* (also known as monocyte chemoattractant protein; which plays a role in monocyte recruitment<sup>4,53</sup>) and *Ccl11* (which plays a role in eosinophil recruitment<sup>54</sup>), in the GEO datasets (GSE41667 and GSE79592) explains the higher influx of alveolar macrophages and eosinophils, respectively, that were observed in the chronic AAD model. Our findings that infiltrating CD206<sup>+</sup> macrophages associated with a M2 phenotype and resident CD68<sup>+</sup> alveolar macrophages were specifically involved in the uptake of NP-RLX is likely explained by the abundance (Supplementary Figure 4) and phagocytic capacity of these cells that were present in airways of mice with OVA-induced chronic AAD. On the other hand, the RLX-induced reduction of CCL11 would have resulted in reduced eosinophil infiltration, and the lack of any NP-RLX uptake by the latter, as they do not undergo phagocytosis.

The glycoprotein, CD68, has been reported as a pan-macrophage/dendritic cell marker<sup>30</sup>. We established that lung myeloid cells have different expression levels of CD68 (Hi/Lo), where the CD68<sup>hi</sup> population represented alveolar macrophages, and the CD68<sup>lo</sup> population represented interstitial macrophages<sup>30</sup>. Whilst other markers used to identify macrophages, including F4/80, CD11b and CD11c, are not restricted to macrophages<sup>4</sup>, studies have shown that alveolar macrophages are characterized as CD45<sup>+</sup>/CD68<sup>hi</sup>/F4/80<sup>+</sup>/CD11b<sup>-</sup>/CD11c<sup>+</sup> cells, whereas CD45<sup>+</sup>/CD68<sup>lo</sup>/F4/80<sup>+</sup>/CD11b<sup>+</sup>/CD11c<sup>+</sup>, CD45<sup>+</sup>/CD68<sup>lo</sup>/F4/80<sup>+</sup>/CD11b<sup>+</sup>/CD11c<sup>-</sup> and CD45<sup>+</sup>/CD68<sup>-</sup>/F4/80<sup>-</sup>/CD11b<sup>+</sup>/Gr1<sup>hi</sup> cells are used to characterize interstitial macrophages, monocytes and neutrophils, respectively<sup>30</sup>. Using these cell characteristics, we identified the uptake of NP-

RLX by CD206<sup>+</sup>/F4/80<sup>+</sup>/CD11c<sup>+</sup> (alveolar M2 macrophages), CD68<sup>hi</sup>/F4/80<sup>+</sup>/CD11b<sup>-</sup>/CD11c<sup>+</sup> (pulmonary monocyte/macrophages) and CD68<sup>lo</sup>/F4/80<sup>+</sup>/CD11b<sup>+</sup>/CD11c<sup>+</sup> (resident interstitial macrophages) cells.

The OVA-induced chronic AAD model has often been used to evaluate different therapies for the treatment of asthma<sup>11,14</sup>, as it presents with the central features of human asthma<sup>31</sup>. The use of SPIONs to generate NP-RLX not only provided a sustained therapeutic effect of RLX as a treatment for chronic AAD/asthma, but also allowed for the dose-dependent effects of the hormone-drug to be delineated. Notably, intranasal dosing of NP-RLX Hi (25ng/ml) showed comparable therapeutic efficacy to continuous systemic (Pump)-RLX treatment of mice (which produced similar circulating levels of RLX). NP-RLX was also delivered at a 5-fold lower dose (5 ng/ml), which is slightly higher than circulating levels (of up to ~1-2 ng/ml) found in pregnant women undergoing single pregnancies<sup>39</sup>. NP-RLX Lo still exerted anti-inflammatory and anti-remodelling effects that reduced OVA-induced AHR and recovery of the loss of dynamic lung compliance, comparable to NP-RLX Hi and Pump-RLX treatment. This is somewhat consistent with our previous findings<sup>14,15,25</sup> which have demonstrated that therapies that effectively reduce airway/lung fibrosis, and to a lesser degree epithelial damage and thickening (as part of AWR), correspondingly reduce AHR; and to a greater extent over therapies that only reduce AI.

The findings of this study also revealed insights into RLX's protective mechanisms of action in the context of chronic AAD, and provided evidence supporting its potential therapeutic benefit in opposing fibrosis in human asthma (see Supplementary Figure 10). RLX treatment *in vivo* inhibited AI by reducing OVA-induced CCL11 and CCL2 levels (which recruit eosinophils and macrophages to infiltrate damaged tissues) as well as the expression of the pro-inflammatory cytokines, IL-1 $\beta$ , IL-6 and TNF- $\alpha$  in mice with chronic AAD. It had been previously suggested

that RLX could inhibit the production of these three inflammatory cytokines by human macrophages, via an interaction with the glucocorticoid receptor<sup>55</sup>. Furthermore, as IL-1 $\beta$  is produced by the NLRP3 inflammasome, which is expressed by a number of cells including macrophages and (myo)fibroblasts<sup>56</sup>, it is possible that the inhibitory effects of NP-RLX on IL-1 $\beta$  were mediated through its ability to inhibit NLRP3 inflammasome priming and/or activity<sup>57-59</sup>. Interestingly, while daily intranasal administration of (unconjugated) RLX alone did not affect the OVA-induced goblet cell metaplasia<sup>15</sup>, its conjugation to SPIONS (NP-RLX) was able to markedly reduce the number of these mucin-producing cells, suggesting that only sustained RLX activity (which was maintained by NP-RLX) was able to regulate goblet cell metaplasia and other related Th2-mediated processes. Additionally, by reducing macrophage numbers and their ability to produce TGF- $\beta$ 1 and/or directly suppressing epithelial TGF- $\beta$ 1 expression and its signal transduction at the level of Smad2 phosphorylation<sup>60,61</sup>, NP-RLX was likely able to suppress the pro-fibrotic influence of TGF- $\beta$ 1 on myofibroblast differentiation and the subsequent impact of airway fibrosis on airway resistance and dynamic lung compliance. Further support for the anti-fibrotic potential of NP-RLX was obtained from its inhibitory effects on TGF- $\beta$ 1-induced contraction of collagen gels and collagen I deposition from myofibroblasts derived from asthmatic patients. Thus, we provide compelling evidence that NP-RLX may represent a stand-alone means of reducing AI, AWR and AHR through specific macrophage subsets. Future studies exploring extended treatment periods of chronic AAD with NP-RLX and related mimetics<sup>62,63</sup> will provide insights into its potential clinical application as a treatment for human asthma.

## CONCLUSION

In conclusion, we have demonstrated that SPIONS provide a novel vehicle for delivering therapeutic agents into chronically inflamed and remodeled airways, and were able to maintain the



efficacy of RLX activity, when administered every 48 hours over a 1-week treatment period. We also showed that NP-RLX was largely taken up by infiltrating alveolar M2 macrophages and resident interstitial macrophages, and when intermittently-administered into the inflamed airways of mice, was able to maintain the same therapeutic efficacy in partially reversing the established chronic AAD-induced AI, AWR, fibrosis and AHR *in vivo*, as systemically-infused Pump-RLX which required continuous application to maintain efficacy. Furthermore, NP-RLX was able to prevent human asthmatic patient-derived lung myofibroblasts from undergoing TGF- $\beta$ 1-stimulated collagen gel contraction and collagen I deposition to the same extent as RLX, further highlighting the clinical application of NP-RLX as a viable treatment for asthmatics. Based on its anti-remodelling and anti-fibrotic effects, NP-RLX may represent a stand-alone means of treating the 5-10% of asthmatics that are resistant to corticosteroid therapy, or may be used as an adjunct therapy to clinically-used corticosteroids (that mainly target AI and the contribution of AI to AHR) to more completely treat the three central pathological components of asthma.

## Supporting Information

The manuscript contains a single compiled file as supporting information that contains the following: (i) Supplementary Table 1: Concentration of RLX conjugated on SPIONs measured using Quantikine H2- Relaxin ELISA; (ii) Supplementary Figure 1: The concentration of RLX conjugated to SPIONs were evaluated using the Quantikine H2 relaxin ELISA; (iii) Supplementary Figure 2: Lung dry weight, schematic illustration of LPS induced acute lung injury and OVA induced chronic AAD; (iv) Supplementary Figure 3: Perl's Prussian Blue staining of the extent of NP-RLX vs NP-empty uptake by macrophages vs neutrophils, respectively; (v) Supplementary Figure 4: Immunohistochemical staining of M2 vs M1 macrophages in the airways of saline vs OVA sensitized and challenged mice; (vi) Figure 5: Serum RLX levels from OVA sensitized and challenged mice treated with pump-RLX, NP-RLX or NP-Empty; (vii) Supplementary Figure 6: Representative immunohistochemical-stained lung sections from each of the groups studied, for the proinflammatory cytokines; (viii) Supplementary Figure 7: Representative immunohistochemical-stained lung sections from each of the groups studied for TSLP, TGF- $\beta$ 1 and pSmad2; (ix) Supplementary Figure 8: Representative immunohistochemical-stained lung sections from each of the groups studied show the extent of  $\alpha$ -SMA-stained; (x) Supplementary Figure 9: Collagen I deposition from TGF- $\beta$ 1-stimulated human lung myofibroblasts derived from human asthmatic patients, treated with 5, 25 or 60ng/ml of RLX vs NP-RLX; and (xi) Supplementary Figure 10: A schematic illustration of the main findings of this study, outlining the proposed mechanisms by which NP-RLX was inducing its therapeutic effects in the setting of chronic AAD/asthma.

## **Author Contribution**

A.C., C.S., and C.S.S designed the research; A.C., A.A.P., M.L., J.B., S.G.R., C.S., and C.S.S performed all experiments or contributed reagents and tools; A.C., A.A.P., M.L., J.B., S.G.R., C.S., and C.S.S analyzed the data; All authors contributed to preparation of the manuscript.

## **Funding Sources**

This work was in part funded by an Australian Research Council (ARC) Future (Research) Fellowship and Discovery Project Grant (DP150101058) to C. Selomulya; a Monash Biomedicine Discovery Institute Senior Research Fellowship to C. Samuel; and a National Health and Medical Research Council (NHMRC) of Australia Project Grant (GNT1165690) to J. Bourke and S. Royce.

## **Acknowledgements**

The authors acknowledge the following Monash University research platforms for providing scientific and technical assistance: Monash Centre for Electron Microscopy (MCEM), Monash University Imaging Platform, Monash University FlowCore Platform, and Monash University Histology platform. The authors also thank Prof. Philip Bardin and Dr Belinda Thomas (Hudson Institute of Medical Research, Melbourne, Victoria, Australia) for providing the primary human lung fibroblasts from asthmatic vs non-asthmatic patients.

**Data sharing:** The data that supports the findings of this study are also available from the corresponding authors upon reasonable request. Some data may not be available because of privacy or ethical restrictions.

## ABBREVIATIONS

$\alpha$ -SMA,  $\alpha$ -smooth muscle actin; AAD, allergic airways disease; ABPAS, Alcian blue-Periodic acid Schiffs staining; ACK, ammonium chloride potassium; AI, airway inflammation; AHR, airway hyperresponsiveness; AWR, airway remodeling; BALF, bronchoalveolar lavage fluid; BM, basement membrane; CCL, chemokine C-C motif ligand; CHN, carbon nitrogen and Hydrogen; DAPI, 4',6-diamidino-2-phenylindole; ECM, extra-cellular matrix; EDC, N-(3-Dimethylaminopropyl)-N'-ethylcarbodiimide hydrochloride; EDTA, ethylene-diamine tetra acetic acid; FACS, fluorescence-assisted cell sorting; FBS, fetal bovine serum; FEGTEM, field emission gun transmission electron microscopy; FITC, fluorescein isothiocyanate; FTIR, fourier transformed infrared radiation; FMO, fluorescent minus one; FSC, forward scatter; GEO, gene expression omnibus; HPLC, High performance liquid chromatography; LPS, lipopolysaccharide; MCP-1, monocyte chemoattractant protein-1; MEM, minimum essential media; MES, 2-(N-Morpholino) ethanesulfonic acid; NHS, N-Hydroxysuccinimide; NP, nanoparticle; NP-RLX, (se)relaxin-conjugated nanoparticles; OVA, ovalbumin; pDI, poly-dispersity index; RLX, (se)relaxin; RXFP1, Relaxin Family Peptide Receptor 1; SDS-PAGE, sodium dodecyl sulfate-poly acrylamide gel electrophoresis; SSC, side scatter; TEM, transmission electron microscopy; TGF- $\beta$ 1, transforming growth factor- $\beta$ 1; Th2, T helper 2; TLC, thin layer chromatography; TSLP, thymic stromal lymphopoietin

**KEYWORDS** Asthma, Airway remodeling, Airway hyperresponsiveness, Nanoparticle-conjugated drug delivery, Serelaxin.

## REFERENCES

- 1 Masoli, M., Fabian, D., Holt, S. & Beasley, R. The global burden of asthma: executive summary of the GINA Dissemination Committee report. *Allergy* **59**, 469-478, doi:10.1111/j.1398-9995.2004.00526.x (2004).
- 2 Royce, S. G., Moodley, Y. & Samuel, C. S. Novel therapeutic strategies for lung disorders associated with airway remodelling and fibrosis. *Pharmacol Ther* **141**, 250-260, doi:10.1016/j.pharmthera.2013.10.008 (2014).
- 3 Dharmage, S. C., Perret, J. L. & Custovic, A. Epidemiology of Asthma in Children and Adults. *Frontiers in Pediatrics* **7**, doi:10.3389/fped.2019.00246 (2019).
- 4 Chakraborty, A., Boer, J. C., Selomulya, C., Plebanski, M. & Royce, S. G. Insights into endotoxin-mediated lung inflammation and future treatment strategies. *Expert Rev Respir Med* **12**, 941-955, doi:10.1080/17476348.2018.1523009 (2018).
- 5 Seumois, G. *et al.* Transcriptional Profiling of Th2 Cells Identifies Pathogenic Features Associated with Asthma. *J Immunol* **197**, 655-664, doi:10.4049/jimmunol.1600397 (2016).
- 6 Lloyd, C. M. & Hessel, E. M. Functions of T cells in asthma: more than just T(H)2 cells. *Nature reviews. Immunology* **10**, 838-848, doi:10.1038/nri2870 (2010).
- 7 Bijl-Hofland, I. D. *et al.* Inhaled Corticosteroids, Combined with Long-acting  $\beta$ 2-Agonists, Improve the Perception of Bronchoconstriction in Asthma. *Am J Respir Crit Care Med* **164**, 764-769, doi:10.1164/ajrccm.164.5.9910103 (2001).
- 8 Brannan, J. D. & Loughheed, M. D. Airway hyperresponsiveness in asthma: mechanisms, clinical significance, and treatment. *Front Physiol* **3**, 460-460, doi:10.3389/fphys.2012.00460 (2012).
- 9 Barnes, P. J. Corticosteroid resistance in patients with asthma and chronic obstructive pulmonary disease. *J Allergy Clin Immunol* **131**, 636-645, doi:10.1016/j.jaci.2012.12.1564 (2013).
- 10 Dahl, R. Systemic side effects of inhaled corticosteroids in patients with asthma. *Respir Med* **100**, 1307-1317, doi:10.1016/j.rmed.2005.11.020 (2006).
- 11 Kenyon, N. J., Ward, R. W. & Last, J. A. Airway fibrosis in a mouse model of airway inflammation. *Toxicol Appl Pharmacol* **186**, 90-100, doi:10.1016/s0041-008x(02)00025-x (2003).
- 12 Bani, D., Ballati, L., Masini, E., Bigazzi, M. & Sacchi, T. B. Relaxin counteracts asthma-like reaction induced by inhaled antigen in sensitized guinea pigs. *Endocrinology* **138**, 1909-1915, doi:10.1210/endo.138.5.5147 (1997).
- 13 Lam, M., Royce, S. G., Samuel, C. S. & Bourke, J. E. Serelaxin as a novel therapeutic opposing fibrosis and contraction in lung diseases. *Pharmacol Ther* **187**, 61-70, doi:10.1016/j.pharmthera.2018.02.004 (2018).
- 14 Royce, S. G. *et al.* Relaxin reverses airway remodeling and airway dysfunction in allergic airways disease. *Endocrinology* **150**, 2692-2699, doi:10.1210/en.2008-1457 (2009).
- 15 Royce, S. G. *et al.* Intranasally administered serelaxin abrogates airway remodelling and attenuates airway hyperresponsiveness in allergic airways disease. *Clin Exp Allergy* **44**, 1399-1408, doi:10.1111/cea.12391 (2014).
- 16 Chen, S. A. *et al.* The pharmacokinetics of recombinant human relaxin in nonpregnant women after intravenous, intravaginal, and intracervical administration. *Pharm Res* **10**, 834-838, doi:10.1023/a:1018901009062 (1993).
- 17 Bathgate, R. A. *et al.* Relaxin family peptides and their receptors. *Physiol Rev* **93**, 405-480, doi:10.1152/physrev.00001.2012 (2013).

- 18 Chen, L. *et al.* Relaxin abrogates renal interstitial fibrosis by regulating macrophage polarization via inhibition of Toll-like receptor 4 signaling. *Oncotarget* **8**, 21044-21053, doi:10.18632/oncotarget.15483 (2017).
- 19 Chakraborty, A., Royce, S. G., Selomulya, C. & Plebanski, M. A novel Approach for Non-Invasive Lung Imaging and Targeting Lung Immune Cells. *Int J Mol Sci* **21**, 1613 (2020).
- 20 Mazuel, F. *et al.* Massive Intracellular Biodegradation of Iron Oxide Nanoparticles Evidenced Magnetically at Single-Endosome and Tissue Levels. *ACS Nano* **10**, 7627-7638, doi:10.1021/acsnano.6b02876 (2016).
- 21 Ghasempour, S., Shokrgozar, M. A., Ghasempour, R. & Alipour, M. Investigating the cytotoxicity of iron oxide nanoparticles in in vivo and in vitro studies. *Exp Toxicol Path* **67**, 509-515, doi:http://dx.doi.org/10.1016/j.etp.2015.07.005 (2015).
- 22 Melgert, B. N. *et al.* Female mice are more susceptible to the development of allergic airway inflammation than male mice. *Clin Exp Allergy* **35**, 1496-1503, doi:10.1111/j.1365-2222.2005.02362.x (2005).
- 23 Chakraborty, A., Royce, S. G., Plebanski, M. & Selomulya, C. Glycine microparticles loaded with functionalized nanoparticles for pulmonary delivery. *Int J Pharm* **570**, 118654, doi:10.1016/j.ijpharm.2019.118654 (2019).
- 24 Masliah, E. *et al.* Passive immunization reduces behavioral and neuropathological deficits in an alpha-synuclein transgenic model of Lewy body disease. *PLoS one* **6**, e19338, doi:10.1371/journal.pone.0019338 (2011).
- 25 Royce, S. G., Mao, W., Lim, R., Kelly, K. & Samuel, C. S. iPSC- and mesenchymoangioblast-derived mesenchymal stem cells provide greater protection against experimental chronic allergic airways disease compared with a clinically used corticosteroid. *FASEB J* **33**, 6402-6411, doi:10.1096/fj.201802307R (2019).
- 26 Chakraborty, A., Royce, S. G., Selomulya, C. & Plebanski, M. A novel Approach for Non-Invasive Lung Imaging and Targeting Lung Immune Cells. *Int J Mol Sci* **21**, doi:10.3390/ijms21051613 (2020).
- 27 Bourke, J. E. *et al.* Collagen remodelling by airway smooth muscle is resistant to steroids and  $\beta$ 2-agonists. *Eur Respir J* **37**, 173-182, doi:10.1183/09031936.00008109 (2011).
- 28 Samuel, C. S. *et al.* Relaxin deficiency in mice is associated with an age-related progression of pulmonary fibrosis. *FASEB J* **17**, 121-123, doi:10.1096/fj.02-0449fje (2003).
- 29 Chakraborty, A. *et al.* Effect of a small natural dietary compound on lung pathology in airway inflammation. *Eur Respir J* **52**, PA1045, doi:10.1183/13993003.congress-2018.PA1045 (2018).
- 30 Zaynagetdinov, R. *et al.* Identification of myeloid cell subsets in murine lungs using flow cytometry. *Am J Respir Cell Mol Biol* **49**, 180-189, doi:10.1165/rcmb.2012-0366MA (2013).
- 31 Foster, P. S. *et al.* Dissociation of inflammatory and epithelial responses in a murine model of chronic asthma. *Lab Invest* **80**, 655-662, doi:10.1038/labinvest.3780068 (2000).
- 32 Locke, N. R., Royce, S. G., Wainwright, J. S., Samuel, C. S. & Tang, M. L. Comparison of airway remodeling in acute, subacute, and chronic models of allergic airways disease. *Am J Respir Cell Mol Biol* **36**, 625-632, doi:10.1165/rcmb.2006-0083OC (2007).
- 33 Thomas, S. Y. *et al.* MyD88-dependent dendritic and epithelial cell crosstalk orchestrates immune responses to allergens. *Mucosal Immunol* **11**, 796-810, doi:10.1038/mi.2017.84 (2018).
- 34 Samuel, C. S. *et al.* Serelaxin Is a More Efficacious Antifibrotic Than Enalapril in an Experimental Model of Heart Disease. *Hypertension* **64**, 315-322, doi:doi:10.1161/HYPERTENSIONAHA.114.03594 (2014).

- 35 Martin, B. *et al.* Relaxin reverses inflammatory and immune signals in aged hearts. *PLoS one* **13**, e0190935, doi:10.1371/journal.pone.0190935 (2018).
- 36 Mu, K. *et al.* Monoclonal antibody-conjugated superparamagnetic iron oxide nanoparticles for imaging of epidermal growth factor receptor-targeted cells and gliomas. *Mol Imaging* **14**, doi:10.2310/7290.2015.00002 (2015).
- 37 Veisoh, O., Gunn, J. W. & Zhang, M. Design and fabrication of magnetic nanoparticles for targeted drug delivery and imaging. *Adv Drug Deliv Rev* **62**, 284-304, doi:10.1016/j.addr.2009.11.002 (2010).
- 38 Chakraborty, A., Boer, J. C., Selomulya, C. & Plebanski, M. Amino Acid Functionalized Inorganic Nanoparticles as Cutting-Edge Therapeutic and Diagnostic Agents. *Bioconjug Chem* **29**, 657-671, doi:10.1021/acs.bioconjchem.7b00455 (2018).
- 39 Bell, R. J. *et al.* Relaxin in human pregnancy serum measured with an homologous radioimmunoassay. *Obstet Gynecol* **69**, 585-589 (1987).
- 40 Dua, K. *et al.* Targeting Chronic Inflammatory Lung Diseases Using Advanced Drug Delivery Systems. (2020).
- 41 Unemori, E. N. *et al.* Relaxin induces an extracellular matrix-degrading phenotype in human lung fibroblasts in vitro and inhibits lung fibrosis in a murine model in vivo. *J Clin Invest* **98**, 2739-2745, doi:10.1172/jci119099 (1996).
- 42 Danielson, L. A. & Conrad, K. P. Time course and dose response of relaxin-mediated renal vasodilation, hyperfiltration, and changes in plasma osmolality in conscious rats. *J Appl Physiol (1985)* **95**, 1509-1514, doi:10.1152/jappphysiol.00545.2003 (2003).
- 43 Sarwar, M., Samuel, C. S., Bathgate, R. A., Stewart, D. R. & Summers, R. J. Serelaxin-mediated signal transduction in human vascular cells: bell-shaped concentration-response curves reflect differential coupling to G proteins. *Br J Pharmacol* **172**, 1005-1019, doi:10.1111/bph.12964 (2015).
- 44 Hoare, B. L. *et al.* Multi-Component Mechanism of H2 Relaxin Binding to RXFP1 through NanoBRET Kinetic Analysis. *iScience* **11**, 93-113, doi:10.1016/j.isci.2018.12.004 (2019).
- 45 van Rijt, S. H., Bein, T. & Meiners, S. Medical nanoparticles for next generation drug delivery to the lungs. *Eur Respir J* **44**, 765-774, doi:10.1183/09031936.00212813 (2014).
- 46 Holgate, S. T. The airway epithelium is central to the pathogenesis of asthma. *Allergol Int* **57**, 1-10, doi:10.2332/allergolint.R-07-154 (2008).
- 47 Wiebert, P. *et al.* Negligible clearance of ultrafine particles retained in healthy and affected human lungs. *Eur Respir J* **28**, 286-290, doi:10.1183/09031936.06.00103805 (2006).
- 48 Möller, W. *et al.* Deposition, retention, and translocation of ultrafine particles from the central airways and lung periphery. *Am J Respir Crit Care Med* **177**, 426-432, doi:10.1164/rccm.200602-301OC (2008).
- 49 Nyberg, K., Johansson, U., Johansson, A. & Camner, P. Phagolysosomal pH in alveolar macrophages. *Environ Health Perspect* **97**, 149-152, doi:10.1289/ehp.9297149 (1992).
- 50 Bidani, A., Brown, S. E., Heming, T. A., Gurich, R. & Dubose, T. D., Jr. Cytoplasmic pH in pulmonary macrophages: recovery from acid load is Na<sup>+</sup> independent and NEM sensitive. *Am J Physiol* **257**, C65-76, doi:10.1152/ajpcell.1989.257.1.C65 (1989).
- 51 Eliopoulos, A. G., Dumitru, C. D., Wang, C. C., Cho, J. & Tschlis, P. N. Induction of COX-2 by LPS in macrophages is regulated by Tpl2-dependent CREB activation signals. *EMBO J* **21**, 4831-4840, doi:10.1093/emboj/cdf478 (2002).
- 52 Feng, X. *et al.* Lipopolysaccharide inhibits macrophage phagocytosis of apoptotic neutrophils by regulating the production of tumour necrosis factor  $\alpha$  and growth arrest-specific gene 6. *Immunology* **132**, 287-295, doi:10.1111/j.1365-2567.2010.03364.x (2011).

- 53 Conti, P. & DiGioacchino, M. MCP-1 and RANTES are mediators of acute and chronic inflammation. *Allergy Asthma Proc* **22**, 133-137, doi:10.2500/108854101778148737 (2001).
- 54 Ravensberg, A. J. *et al.* Eotaxin-2 and eotaxin-3 expression is associated with persistent eosinophilic bronchial inflammation in patients with asthma after allergen challenge. *The J Allergy Clin Immunol* **115**, 779-785, doi:10.1016/j.jaci.2004.11.045 (2005).
- 55 Dschietzig, T., Bartsch, C., Stangl, V., Baumann, G. & Stangl, K. Identification of the pregnancy hormone relaxin as glucocorticoid receptor agonist. *FASEB J* **18**, 1536-1538, doi:10.1096/fj.03-1120fje (2004).
- 56 Pinar, A. A. *et al.* Targeting the NLRP3 inflammasome to treat cardiovascular fibrosis. *Pharmacol Ther* **209**, 107511, doi:10.1016/j.pharmthera.2020.107511 (2020).
- 57 Valle Raleigh, J. *et al.* Reperfusion therapy with recombinant human relaxin-2 (Serelaxin) attenuates myocardial infarct size and NLRP3 inflammasome following ischemia/reperfusion injury via eNOS-dependent mechanism. *Cardiovasc Res* **113**, 609-619, doi:10.1093/cvr/cvw246 (2017).
- 58 Cáceres, F. T., Gaspari, T. A., Samuel, C. S. & Pinar, A. A. Serelaxin inhibits the profibrotic TGF- $\beta$ 1/IL-1 $\beta$  axis by targeting TLR-4 and the NLRP3 inflammasome in cardiac myofibroblasts. *FASEB J* **33**, 14717-14733, doi:10.1096/fj.201901079RR (2019).
- 59 Pinar, A. A., Yuferov, A., Gaspari, T. A. & Samuel, C. S. Relaxin Can Mediate Its Anti-Fibrotic Effects by Targeting the Myofibroblast NLRP3 Inflammasome at the Level of Caspase-1. *Front Pharmacol* **11**, 1201, doi:10.3389/fphar.2020.01201 (2020).
- 60 Heeg, M. H. *et al.* The antifibrotic effects of relaxin in human renal fibroblasts are mediated in part by inhibition of the Smad2 pathway. *Kidney Int* **68**, 96-109, doi:10.1111/j.1523-1755.2005.00384.x (2005).
- 61 Mookerjee, I. *et al.* Relaxin inhibits renal myofibroblast differentiation via RXFP1, the nitric oxide pathway, and Smad2. *FASEB J* **23**, 1219-1229, doi:10.1096/fj.08-120857 (2009).
- 62 Xiao, J. *et al.* in *Probe Reports from the NIH Molecular Libraries Program* (National Center for Biotechnology Information (US), 2010).
- 63 Hossain, M. A. *et al.* A single-chain derivative of the relaxin hormone is a functionally selective agonist of the G protein-coupled receptor, RXFP1. *Chem Sci* **7**, 3805-3819, doi:10.1039/c5sc04754d (2016).



## FIGURE LEGENDS

**Figure 1:** Conjugation and characterization of serelaxin (RLX)-conjugated iron oxide nanoparticles (NP-RLX). Schematic diagram showing conjugation of RLX to carboxyl modified iron oxide nanoparticles using carbodiimide chemistry (A). HRTEM images of RLX conjugated iron oxide nanoparticles with size  $6.9\pm 3.2$  nm (shown in brown with false color imaging) while the conjugated RLX surrounds the nanoparticles (shown in green with false color imaging- inset) (B). The SAED pattern of the nanoparticles confirmed its crystallinity and based on phase calculations the core of the nanoparticles was confirmed to be  $\gamma$ -Fe<sub>2</sub>O<sub>3</sub> as previously developed by us<sup>23,26</sup> (inset-i). FTIR spectra of the nanoparticles validated the conjugation of RLX represented by a blue shift (C). The hydrodynamic size of the nanoparticles was measured for the size of the particles in solution which was  $75.57\pm 4.2$  nm with a PDI 0.155 indicating good colloidal stability (D). The charge of the particles (zeta-potential) was also measured to confirm the conjugation of RLX and was calculated as  $-47.3\pm 12.2$  mV, confirming the conjugation of RLX on the iron oxide nanoparticles (E). The data represented are representatives of 8 experiments conducted and selected randomly for representation.

**Figure 2:** Selective uptake of NP-RLX by alveolar macrophages under inflammatory conditions. To investigate cellular uptake of NP-RLX in the lung, mice were administered intranasal LPS on day 1, then NP-RLX-FITC tagged particles by the same route on day 2, before BALF was collected 2 days later (see supplementary information Figure 2B). Acute Lung Injury (ALI) was validated by elevated levels of neutrophils and alveolar macrophages confirmed by Diff Quik staining (A). The core of the nanoparticles (iron oxide-  $\gamma$ Fe<sub>2</sub>O<sub>3</sub>) was stained with Perl's Prussian blue (B) and the stain was visible only on alveolar macrophages (inset -i) but not on neutrophils (inset-ii). Cells in the BALF were stained with DAPI (blue) representing the nucleus. The NP-RLX (green) was localised in the cytoplasm of alveolar macrophages only and was not found in other immune cells

(C). The uptake of NP-RLX was dependent on the cell diameter (D) and the area of the cell with LPS stimulated mice having higher cell diameter and hence an increased cell area. Upon normalization of cell area, LPS stimulated cells had higher fluorescence intensity/area indicating higher uptake of NP-RLX compared to saline. Scale bar denotes 50  $\mu\text{m}$  in all images.

**Figure 3:** Separation of myeloid cell subsets in the lungs according to CD206 expression. Gating strategy showing lavage cells (FSC-A and SSC-A) followed by doublet exclusion based on FSC-A and FSC-H. Live cells were gated based on the Live/Dead exclusion dye (zombie-V450) where positive staining indicated dead cells (A). All gating had been performed on FMO controls and unstained cells. Based on the live cells, M1 and M2 macrophages were gated on the basis of F4/80 and CD206 surface markers to evaluate for NP-RLX uptake (B); NP-RLX uptake was based on CD206 by CD11c<sup>pos</sup> cells (C) and CD68<sup>pos</sup> cells (D). Uptake of NP-RLX by different subsets of CD11c<sup>pos</sup> myeloid progenitors (E). The negative control consisted of Fluorescent Minus One (FMO) controls without Zombie (Live/Dead) marker and unstained controls. The graphs are presented as the means  $\pm$  SDs of four mice treated with NP-RLX followed by lavage after 24 hours. For each flow-plot a representative plot is demonstrated. The histogram shows the FMO control (in green with area shaded) while each of the lavage cells collected from 4 different mice (biological replicates) are represented as different coloured lines. The mean fluorescent intensity (MFI) was quantified in each population of cells and compared in between using un-paired T test with Kruskal Wallis Post-hoc test. \* $P < 0.05$ , \*\* $P < 0.01$ , when comparing the two populations of cells.

**Figure 4:** Separation of myeloid cell subsets in the lungs according to CD68 expression. (A) Flowcytometry plot for differentiating various CD68 subsets of myeloid cells in the lung based on FSC-A. In the two subsets of CD68<sup>pos</sup> cells (B) shows the CD68<sup>hi</sup> subset categorised based on the

expression of F4/80 and CD11c. The data shows a higher uptake of NP-RLX by F4/80<sup>pos</sup> cells than that of F4/80<sup>neg</sup> subset under CD11c<sup>pos</sup> cells. Another subset of the CD68<sup>hi</sup> cells, the CD11c<sup>neg</sup>F4/80<sup>pos</sup> cells showed negligible uptake; inferring the requirement of both CD11c and F4/80 for uptake of the NP-RLX. (C) CD68<sup>lo</sup> subset of myeloid cells were categorised by their expression of F4/80 and CD11c. The uptake of NP-RLX was found higher in F4/80<sup>pos</sup> cells than F4/80<sup>neg</sup> cells under the CD11c<sup>pos</sup> subset. However, in another subset of CD11c<sup>neg</sup>F4/80<sup>pos</sup> cells there was negligible uptake of NP-RLX; inferring again the requirement of CD11c for uptake of NP-RLX. The graphs are presented as the means  $\pm$  SDs of four mice treated with NP-RLX followed by lavage after 24 hours. For each flow-plot a representative plot is demonstrated. The histogram shows the FMO control (in green with area shaded) while each of the lavage cells collected from 6 different mice (biological replicates) are represented as different coloured lines. The mean fluorescent intensity (MFI) was quantified in each population of cells and compared in between using un-paired T test with Kruskal Wallis Post-hoc test. **\*\* $P < 0.01$**  compared to F4/80<sup>pos</sup>/CD11c<sup>neg</sup> cells.

**Figure 5:** The effects of NP-RLX vs Pump-RLX on chronic AAD-induced airway inflammation and influx of immune cells in the lung. Representative images of H&E-stained lung sections from mice subjected to OVA-induced chronic AAD and the various treatment strategies investigated (A) demonstrate the extent of inflammatory cell infiltration within the bronchial wall. Also shown is the OVA-induced peribronchial inflammation score, as mean  $\pm$  SD (B) from five airways per mouse – where sections were scored based on the number and distribution of inflammatory cell aggregates on a scale of 0 (no visible inflammation) to 4 (severe inflammation); N=8 animals per group. Also shown are the total (C) and differential BAL fluid cell counts, including eosinophils (D), neutrophils (E), lymphocytes (F) and macrophages (G). Representative images of ABPAS-stained lung sections from mice subjected to OVA-induced chronic AAD and the various treatment

investigated (H) demonstrate the extent of goblet cell metaplasia (inset) within the airways (indicated black arrows). Also shown is the mean  $\pm$  SD number of goblet cells per 100- $\mu$ m BM length, as mean  $\pm$  SEM, induced by OVA (I); N=8 animals per group. \*P<0.05, \*\*P<0.01, \*\*\*P<0.001 vs the saline-treated (control) group; #P<0.05, ##P<0.01, ###P<0.001 vs the OVA alone group; ¶P<0.05, ¶¶P<0.01, ¶¶¶P<0.001 vs OVA+NP-RLX Lo-treated group; §P<0.05, §§P<0.01, §§§P<0.001 vs the OVA+NP-empty- treated group.

**Figure 6:** Expression of airway/lung pro-inflammatory cytokine expression. A volcano plot of differential gene expression in RNA-seq between: (A) saline vs OVA sensitized and challenged murine lungs (n = 6 independent biological samples per group) re-analyzed to identify genes of interest (Gene Expression Omnibus accession no. GSE41667); and between (B) saline vs OVA sensitized and challenged murine lung alveolar macrophages (n=3 independent biological samples per group) re-analyzed to identify genes of interest (Gene Expression Omnibus accession no. GSE79592<sup>33</sup>). Significantly differentially expressed genes are on the quadrants above ( $-\log_{10}P>2$ ) with specific labelled genes of interest representing pro-inflammatory cytokines, fibrotic markers and Th2-cell attractant chemokines (*Ccl2*-macrophages and *Ccl11*-eosinophils) are represented on the first quadrant. (C) Heat map representing differential gene expression from the inflamed heart tissue of aged (24 months)-female rats treated with or without RLX; re-analyzed to identify genes of interest (Gene Expression Omnibus accession no. GSE106337<sup>35</sup>). A significant reduction in pro-inflammatory genes and fibrotic markers was found in RLX-treated rats in comparison to inflammatory controls. Also shown are the mean  $\pm$  SD staining expression levels of IL-1 $\beta$  (D), IL-6 (E) and TNF- $\alpha$  (F); and BALF expression levels of CCL2/MCP-1 (G) and CCL11/Eotaxin-1 (H) in each of the groups studied; from N=8 mice per group. \*P<0.05, \*\*\*P<0.001 vs the saline-treated (control) group; #P<0.05, ###P<0.001 vs the OVA alone group; +P<0.05 vs OVA+NP-RLX

Hi-treated group; <sup>¶¶¶</sup>P<0.001 vs OVA+NP-RLX Lo-treated group; <sup>§§§</sup>P<0.001 vs the OVA+NP-empty- treated group.

**Figure 7:** The effects of NP-RLX vs Pump-RLX on chronic AAD-induced AWR, fibrosis and airway/lung function. Representative images of Masson's trichrome-stained lung sections from mice subjected to OVA-induced chronic AAD and the various treatment investigated (A) demonstrate the extent of airway epithelial thickening and subepithelial ECM/collagen deposition around the airways in each of the groups. Also shown is the mean  $\pm$  SD airway epithelial thickness (B); and subepithelial ECM deposition (C); from five airways per mouse; N= 8 animals per group; as is the extent (mean  $\pm$  SD) of immunohistochemically-stained TSLP-associated epithelial damage (D); epithelial TGF- $\beta$ 1 expression (E); epithelial (nuclear) pSmad2 (F) and subepithelial myofibroblast accumulation (G). The effects of NP-RLX vs Pump-RLX on chronic AAD-induced airway reactivity (AHR) in response to increasing concentrations of methacholine (H) and mean  $\pm$  SD dynamic lung compliance (at the highest dose of methacholine tested (50ng/ml) (I) demonstrated the extent of airway/lung function in each groups studied; from N = 8 mice per group. \*P<0.05, \*\*P<0.01, \*\*\*P<0.001 vs the saline-treated (control) group; #P<0.05, ##P<0.01, ###P<0.001 vs the OVA alone group; <sup>†</sup>P<0.05 vs OVA+Pump-RLX-treated group; <sup>+</sup>P<0.05 vs OVA+NP-RLX Hi-treated group; <sup>¶</sup>P<0.05, <sup>¶¶</sup>P<0.01 vs OVA+NP-RLX Lo-treated group; <sup>§</sup>P<0.05, <sup>§§</sup>P<0.01 vs the OVA+NP-empty- treated group.

**Figure 8:** TGF- $\beta$ 1-induced contraction in gels seeded with asthmatic fibroblasts is inhibited by NP-relaxin Hi. The effect of TGF- $\beta$ 1 and NP-empty (vehicle control) on collagen gel contraction over 48 hours was assessed in gels seeded with non-asthmatic (A) and asthmatic airway fibroblasts (B). Representative images demonstrate changes in gel area where white dotted circle= initial gel area, white circle= gel area (C). The effect of RLX, NP-RLX-Lo and NP-RLX Hi on collagen gel

contraction in the presence of TGF- $\beta$ 1 were assessed in gels seeded with non-asthmatic (D) and asthmatic fibroblasts (E). Data in time-dependent curves is expressed as % initial area. Data for treatments at 48h (bar graphs) are presented as % contraction (duplicates for n= 3 non-asthmatic; n= 3 asthmatic).